Influence of Rebar Diameter in Concrete Cracking Studied Using a Discrete Crack Approach

Daniel Dias-da-Costa[1] and Rui Graça-e-Costa[2]
[1]School of Civil Engineering, The University of Sydney, 2006 NSW, Australia
[2]CEPAC, University of Algarve, Campus de Gambelas, 8005-139 Faro, Portugal.

Abstract: The ability to model fracture propagation is critical to predict the structural response of a concrete member and possible failure mechanisms. Even for structures under normal service loads, good estimations on the overall deflections and associated stiffness are highly dependent on the onset of fracture and resulting crack pattern, both directly related with the tension-stiffening effect. With the aim of developing robust models to capture this behaviour, a preliminary numerical study is herein presented on the influence of rebar diameter in the cracking pattern of concrete beams captured numerically. Focus is first given to the performance of the numerical model and its mesh objectivity. Experimental results from concrete beams tested under flexural loads are adopted for validation. Two very distinct rebar diameters are used to assess the ability of the model in predicting the average crack opening, maximum crack opening and average crack spacing for a wide range of loads.

Keywords: Discrete crack models, crack pattern, validation.

1. Introduction

It is well-known that reinforced concrete structures are typically cracked even for relatively small service loads. Quantifying the damage associated with any given load level is essential to predict the overall behaviour of the structure, including its deflections. This damage depends on the maximum load level ever attained and on the resulting crack pattern. Considerable amount of research was done in terms of numerical modelling of fracture. One of the most commonly used techniques is based on the smeared crack approach, according to which discontinuous fracture is handled on an averaged sense [1-3]. This formulation is very convenient for implementation purposes and provides good results for micro-cracking and diffused crack patterns. Smeared models, however, are unable to simulate true material separation in the presence of the highly localised cracks that often develop in structures, particularly when approaching its ultimate load capacity.

Other existing approaches have tackled material separation directly in the scope of the discrete crack approach [2,4]. Remeshing algorithms, where the underlying finite element mesh is progressively modified with crack propagation [5-7], were shown to be quite effective. The drawback of such approaches is related to the frequent need to modify meshes. Nodal and element enrichment approaches can overcome such shortcomings. At the expense of additional degrees of freedom, enrichment approaches enable the simulation of the discontinuous displacement fields associated with cracks [8-16]. Most research carried out to date, however, focused mainly on the development of the techniques and validation was performed mostly with well-known benchmarks. As finite element enrichment techniques become more available, their limitations and advantages need to be critically assessed at a deeper level, so that they can be employed in the design of structures. Validation should address not only the ability to predict the overall structural behaviour for both service and ultimate loads, but other parameters – e.g. crack patterns and crack openings – have to be correctly predicted as well.

This paper describes a numerical model developed in the context of the discrete crack approach, which can simulate the behaviour of concrete members regardless of the level of damage, from the onset of cracking and until failure. In the following sections, the model is assessed in its performance and mesh objectivity. Experimental results from Pérez Caldentey et al. [17] are used for validation regarding crack openings and average spacing, for a relatively wide range of loads.

2. Numerical approach

The numerical model adopted in this paper uses a technique to embed discontinuities in the finite element mesh and applicable to the simulation of fracture under tensile stresses. The main aspects concerning this formulation, analytical derivations and numerical implementation can be found in [13-16], reason why only the main features are recovered in the following.

According to the concept of the discrete crack approach [18], microcracking is assumed localised into a surface of discontinuity when the tensile strength of the material is reached. The onset of localisation and corresponding load can be identified with the Rankine criterion in the case of quasi-brittle materials. When load increases further, damage progresses and the discontinuity opens gradually while the tensile stress is softened. The load carrying capacity under tension decreases and, since both discontinuity and neighbouring material are in equilibrium, the neighbouring material unloads elastically. A true crack is said to be formed when damage reaches its maximum and the discontinuity is no longer able to withstand tensile stresses.

The opening of the crack can be mathematically formulated by a jump in the displacement field that occurs with the corresponding strain unbounded. The variational principle for a body Ω with an external boundary Γ and a strong discontinuity Γ_d defining two subregions, Ω^+ and Ω^-, can be written as [19]:

$$-\int_{\Omega\setminus\Gamma_d}(\nabla^s\delta\mathbf{u}):\boldsymbol{\sigma}(\boldsymbol{\varepsilon})d\Omega-\int_{\Gamma_d}\delta\ \mathbf{u}\ \cdot\mathbf{t}^+d\Gamma+\int_{\Omega\setminus\Gamma_d}\delta\mathbf{u}\cdot\mathbf{b}d\Omega+\int_{\Gamma_t}\delta\mathbf{u}\cdot\mathbf{t}d\Gamma=0 \tag{1}$$

where $\boldsymbol{\sigma}$ is the stress tensor, $\boldsymbol{\varepsilon}$ is the strain, $\mathbf{u}$ is the total displacement, $\mathbf{t}^+$ is the vector of tractions applied to the discontinuity, $\mathbf{u}$ is the opening of the discontinuity, and $\mathbf{b}$ and $\mathbf{t}$ are, respectively, the body forces and natural boundary conditions.

The total displacement inside the body, $\mathbf{u}$, can be obtained by overlaying the displacement of the uncracked material, $\hat{\mathbf{u}}$, with the displacement caused by the opening of the discontinuity, $\tilde{\mathbf{u}}$:

$$\mathbf{u}(\mathbf{x})=\hat{\mathbf{u}}(\mathbf{x})+\mathrm{H}_{\Gamma_d}\tilde{\mathbf{u}}(\mathbf{x}), \tag{2}$$

where H_{Γ_d} is the standard Heaviside function.

Using the latter equation and assuming the opening of the discontinuity to be transmitted to the neighbouring material as if it were a rigid body movement, the variational principle in Eq. (1) can be simplified in the two variational statements [13,14]:

$$\int_{\Omega\setminus\Gamma_d}(\nabla^s\delta\hat{\mathbf{u}}):\sigma(\varepsilon)d\Omega=\int_{\Omega\setminus\Gamma_d}\delta\hat{\mathbf{u}}\cdot\mathbf{b}d\Omega+\int_{\Gamma_t}\delta\hat{\mathbf{u}}\cdot\mathbf{t}d\Gamma, \tag{3}$$

$$\int_{\Gamma_d}\delta\ \mathbf{u}\ \cdot\mathbf{t}^+d\Gamma=\int_{\Omega^+}\delta\tilde{\mathbf{u}}\cdot\mathbf{b}d\Omega+\int_{\Gamma_{t^+}}\delta\tilde{\mathbf{u}}\cdot\mathbf{t}d\Gamma, \tag{4}$$

Eqs. (3) and (4) can then be discretised independently. The first equation corresponds to the standard principle of virtual work and leads to the usual finite element formulation for an uncracked domain. The second equation is equivalent to the principle of virtual work for a zero-thickness interface element applicable to the simulation of fracture or contact between materials [20]. Although both equations are independent, there is a kinematic compatibility condition – see Eq. (2) – that relates the three displacement fields (i.e. field of total displacements, field of displacements without discontinuity, and field of displacements caused by the opening of the discontinuity). At the finite element level, this condition can be casted as:

$$\mathbf{a}^e=\hat{\mathbf{a}}^e+\underbrace{\mathbf{H}^e_{\Gamma_d}\mathbf{M}^{ek}_w\mathbf{w}^e}_{\tilde{\mathbf{a}}^e}, \tag{5}$$

where $\mathbf{a}^e$ are the total nodal degrees of freedom related to $\mathbf{u}^e$, $\hat{\mathbf{a}}^e$ are the degrees of freedom related to $\hat{\mathbf{u}}$, and $\mathbf{w}^e$ are the enhanced nodal degrees related to the opening of the discontinuity. $\mathbf{M}_w^{ek}$ is a matrix that relates the opening of the discontinuity with the rigid body displacement of the regular nodes of the element, and $\mathbf{H}_{\Gamma_d}^e$ is a diagonal matrix with components equal to '1' for nodal degrees of freedom in Ω^{e+} and '0' otherwise.

Following standard finite element discretisation procedures and using the coupling term in Eq. (5), the following system of equations can be obtained:

$$\begin{bmatrix} \mathbf{K}_{\hat{\mathbf{a}}\hat{\mathbf{a}}}^e & -\mathbf{K}_{\mathbf{aw}}^e \\ -\mathbf{K}_{\mathbf{aw}}^e & \mathbf{K}_{\mathbf{ww}}^e + \mathbf{K}_d^e + \mathbf{K}_p^e \end{bmatrix} \begin{Bmatrix} \mathrm{d}\mathbf{a}^e \\ \mathrm{d}\mathbf{w}^e \end{Bmatrix} = \begin{Bmatrix} \mathrm{d}\hat{\mathbf{f}}^e \\ \mathrm{d}\tilde{\mathbf{f}}^e \end{Bmatrix}, \tag{6}$$

where $\mathbf{K}_{\hat{\mathbf{a}}\hat{\mathbf{a}}}^e = \int_{\Omega^e \setminus \Gamma_d^e} \mathbf{B}^{eT} \mathbf{D}^e \mathbf{B}^e \mathrm{d}\Omega^e$ is the stiffness for the regular finite element, $\mathbf{B}^e$ is the strain-nodal displacement matrix, $\mathbf{D}^e$ is the linearised constitutive matrix for the bulk material, $\mathbf{K}_d^e = \int_{\Gamma_d^e} \mathbf{N}_w^{eT} \mathbf{T}^e \mathbf{N}_w^e \mathrm{d}\Gamma$ is the stiffness of the discontinuity, $\mathbf{T}^e$ is the linearised constitutive matrix for the discontinuity, $\mathbf{K}_{\mathbf{aw}}^e = \mathbf{K}_{\hat{\mathbf{a}}\hat{\mathbf{a}}}^e \mathbf{H}_{\Gamma_d}^e \mathbf{M}_w^{ek}$, $\mathbf{K}_{\mathbf{wa}}^e = \mathbf{K}_{\mathbf{aw}}^{eT}$ and $\mathbf{K}_{\mathbf{ww}}^e = \left(\mathbf{H}_{\Gamma_d}^e \mathbf{M}_w^{ek}\right)^T \mathbf{K}_{\hat{\mathbf{a}}\hat{\mathbf{a}}}^e \mathbf{H}_{\Gamma_d}^e \mathbf{M}_w^{ek}$. The additional term $\mathbf{K}_p^e$ is typically included to enforce proper shear jump transmission along the discontinuity [14] and $\mathrm{d}\tilde{\mathbf{f}}^e = \mathrm{d}\mathbf{f}_w^e - \left(\mathbf{H}_{\Gamma_d}^e \mathbf{M}_w^{ek}\right)^T \mathrm{d}\hat{\mathbf{f}}^e$ is zero if all loads are directly applied at the nodes of the element.

The numerical solution is found using the non-iterative procedure discussed in [21]. During the analysis, new discontinuities are introduced at the centre of the finite element when its first principal stress reaches the tensile strength. Discontinuities are then propagated when the first principal stress at the centre of the element ahead or at the tip reaches the tensile strength of the material. The angles of propagation are orthogonal to the first principal stress and are kept fixed after the onset of localisation. It should be highlighted that in the current implementation only one discontinuity can cross a finite element.

3. Validation

Two beams tested by Pérez Caldentey et al. [17] in a four-point loading scheme are adopted for validating and assessing the performance of the numerical model. The beams have the same cross-section and reinforcement layout, although different rebar diameters: one specimen has four 12 mm steel bars (specimen 12-20-00), whereas the other has four 25 mm bars (specimen 25-20-00). The representation is shown in Figure 1 and it should be highlighted that both specimens have no stirrups at the upper face in the middle span.

The experimental study by Pérez Caldentey et al. [17] aimed at characterising the process of cracking under increasing flexural loading for a range of reinforcement ratios and layouts. The material properties for concrete were 26.9 MPa and 2.14 MPa, respectively the compressive and tensile strengths, whereas the fracture energy can be estimated as 0.050N/mm. The steel had a yielding stress of 550 MPa.

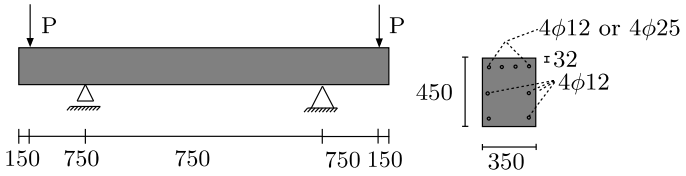

Figure 1. Loading scheme and cross-section (all dimensions in mm).

3.1 Mesh discretisation

Two meshes with different levels of discretisation (one coarse, one refined) are selected for assessing the objectivity of the numerical model – see representation in Figure 2.

Steel reinforcements are simulated using linear elements connected to concrete elements with zero-thickness interfaces. The bond-slip law is given in Model Code 2010 [22], with the onset of slip defined for 0.19 MPa and the ultimate peak bond strength of 10.5 MPa for 0.6 mm slip. The reinforcement is linear elastic and perfectly plastic for both tensile and compressive stresses. The concrete elements are under plane stress conditions, linear elastic under tensile stresses (with embedded cracks being used when the tensile strength of the material is reached) and linear elastic perfectly plastic under compression.

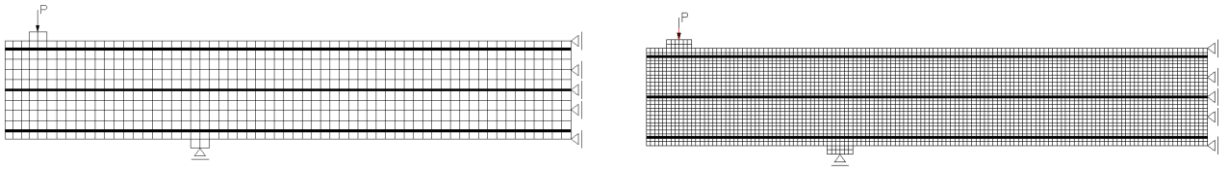

(a) (b)

Figure 2. Meshes with two different levels of discretisation: (a) coarse; and (b) refined.

For comparison, both discretisations are defined using the same material properties, constitutive models and 12 mm reinforcements (see Figure 2). The resulting load vs. displacement curves are compared in Figure 3, together with experimental data found in [23]. It should be mentioned, however, that the available experimental results concern specimen 12-20-10 in [17], which despite having similar material properties and amount of longitudinal reinforcement, also has stirrups. In any case, the experimental results are only shown to provide indicative values, and given that 12-20-10 was not heavily reinforced for shear, the differences are expected to be small, at least for the first stages of damage propagation.

Figure 3 denotes the high degree of proximity between coarse and refined meshes in overall responses. Both models capture well the onset of cracking. The models also capture the behaviour and progressive loss of stiffness with increasing deflection. Results are very close to experimental data.

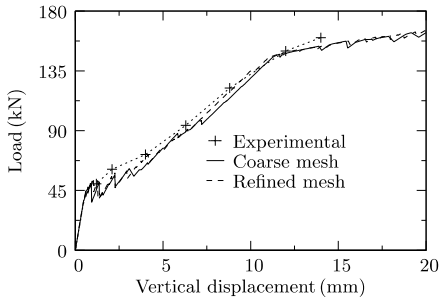

Figure 3. Load vs. vertical displacement curves.

Figure 4 shows the crack pattern obtained with both meshes for three stages of loading, where only cracks with openings above 0.02 mm – i.e., considered to be active – are shown. The crack pattern is relatively similar in both meshes. Since the numerical implementation allows only one discontinuity per finite element, the coarser model shows situations where two or three partial cracks are unable to align and form a single continuous crack. This is particularly noticeable in the mid-span in Figure 4a. The refined mesh does not present such issue.

The average crack spacing depends on the constitutive model adopted for bond-slip. After the first crack is formed and active, the debond between steel and concrete occurs near the crack, which widens progressively with increasing slip. As the distance to the crack increases, the damage and debond

become smaller and the bond transfer mechanism is re-established. The tensile stresses in concrete increase again and conditions can be met for new cracks to localise. This process occurs progressively and secondary cracks form at later stages of loading.

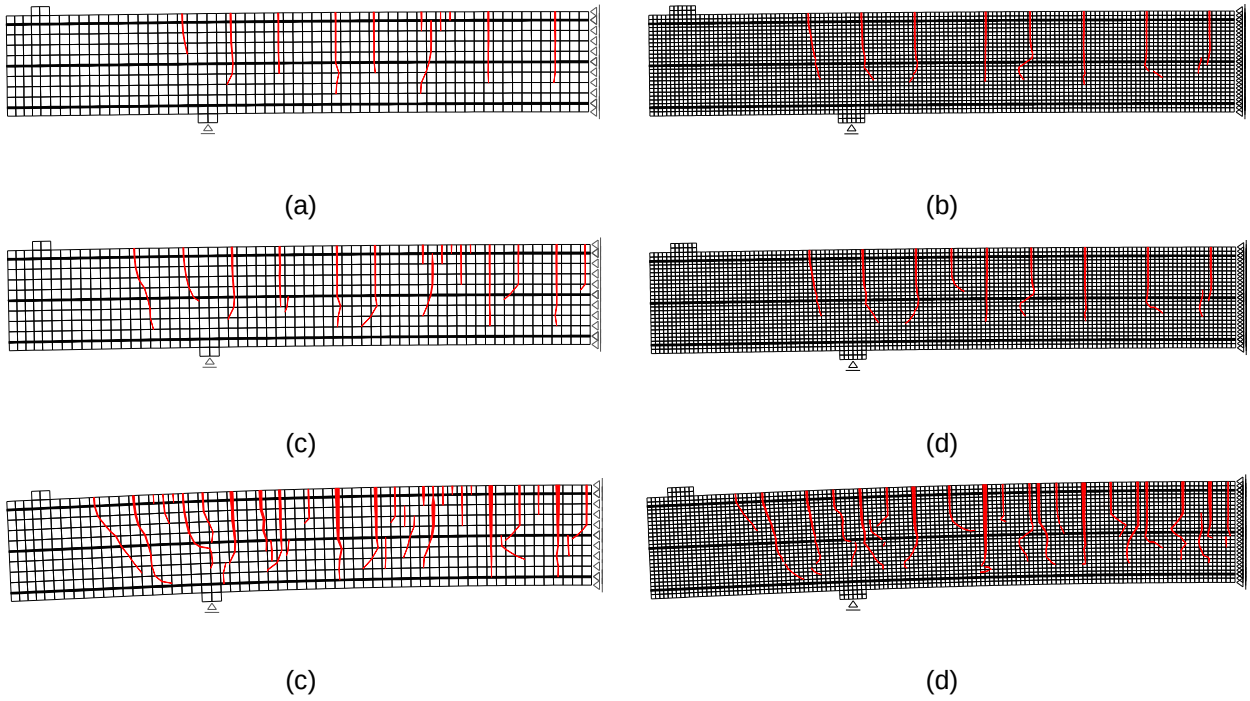

Figure 4. Map showing active cracks for both coarse and refined meshes at: (a) 70kN; (b) 90kN; and at (c) 160 kN.

3.2 Crack spacing and openings

In this section the numerical models are compared with experimental results for average crack opening, maximum crack opening, average crack spacing and final crack distribution. For this study, only the refined mesh is considered. Table 1 summarises the main results and provides experimental data from [17,24].

Table 1. Average crack opening, maximum crack opening and average crack spacing.

		Average crack opening			Maximum crack opening			Average crack spacing		
	Load (kN)	Num. (mm)	Exp. (mm)	error	Num. (mm)	Exp. (mm)	error	Num. (mm)	Exp. (mm)	error
12-20-00	70.1	0.239	0.164	46%	0.271	0.37	-27%	-	-	-
	90.1	0.300	0.243	23%	0.366	0.41	-11%	-	-	-
	160.1*	0.416	0.632	-34%	0.793	0.969	-18%	115	173	-34%
25-20-00	100.0	0.116	0.123	-13%	0.132	0.198	-33%	-	-	-
	180.7	0.156	0.148	-1%	0.213	0.287	-26%	-	-	-
	400.2	0.204	0.352	-33%	0.295	0.688	-57%	86	131	-35%

* the experimental value was measured at 175kN [24].

The average absolute error for the maximum crack opening among all stages and models is 29%, a value that is similar to the one found for the average crack opening (25%). This shows that the numerical models have similar performance regardless of the parameter related to cracking being analysed. It would nevertheless be desirable to compare with experimental data for load vs. displacement curves, to assess if this error can be partially explained by differences in the overall structural behaviour. Such results were not available at the time this article was written.

Although the numerical model apparently tends to underestimate the experimental values, this cannot be assumed as a feature of the model without further testing. In fact, given that the average error is of the same order for all parameters (average and max opening, crack spacing) in Table 1, it is likely to be caused by the choice of constitutive parameters in the simulation rather than by the discrete crack formulation used. The fracture energy was based on typical values and the bond-slip law was taken from Model Concrete 2010 [22]. Since both are highly connected to the process of crack localisation, propagation and opening, they impact the accuracy of the numerical results.

Figure 5 shows the development of cracking for the same load steps in Table 1. This figure highlights that the numerical model captures the changes in crack spacing caused by the different reinforcement diameters, with the smaller average spacing being observed in specimen 25-20-00 at the stabilised stage (see also Table 1).

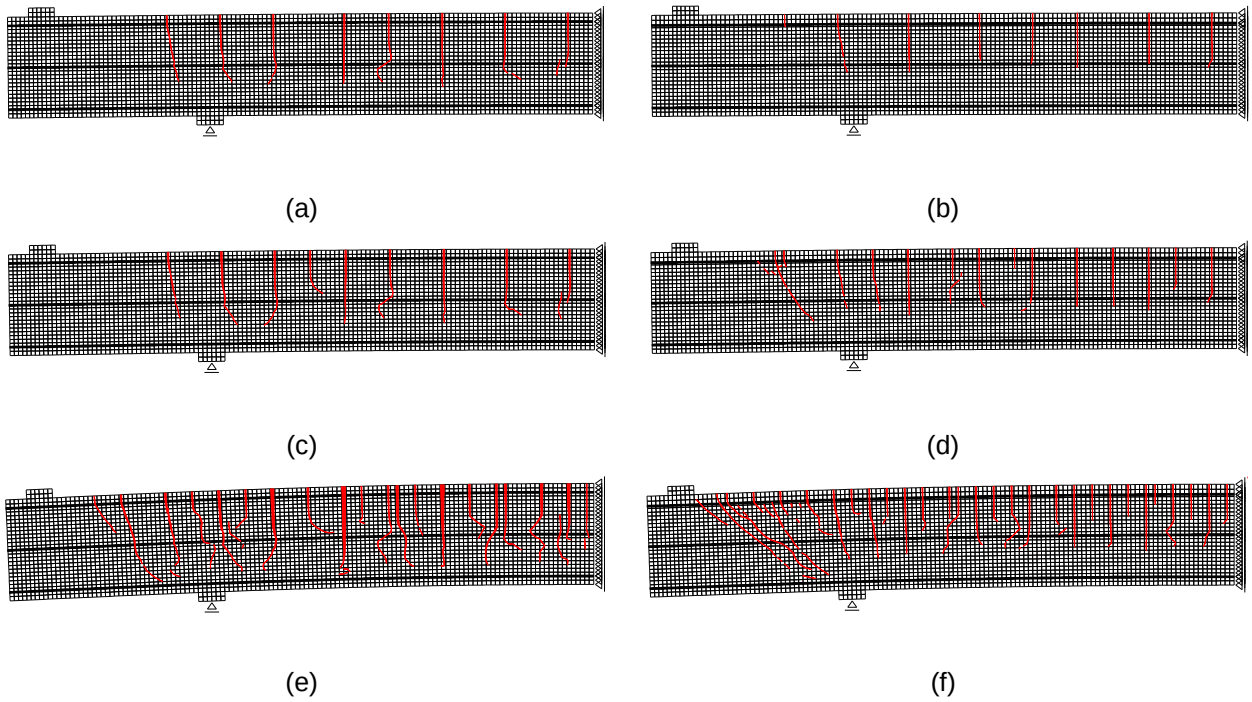

Figure 5. Crack maps for specimens 12-20-00 at: (a) 70kN; (c) 90kN; and (e) 160kN; and 25-20-00 at: (b) 100kN; (d) 180 kN and (f) 400kN.

Figure 6 compares the crack pattern for the last stage of loading in both specimens. The representation of the width is scaled so that relative differences can be easily noticed. The experimental crack map is based on a sketch representation from results and pictures available in [17]. The crack pattern in both numerical models captures all main features observed experimentally, including the number and direction of cracks and openings. The failure of specimen 25-20-00 occurs with the crushing of concrete near the support, as evidenced by the experimental pattern in Figure 6b. Numerically, this behaviour is also observed.

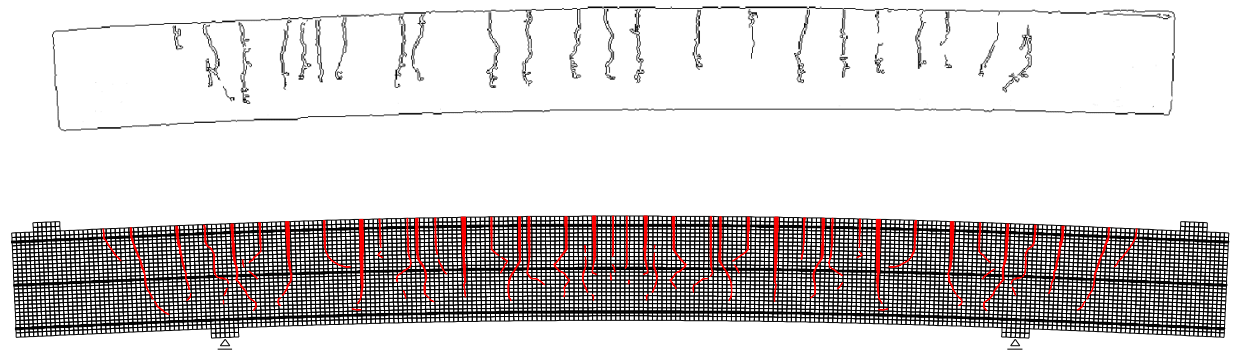

(a)

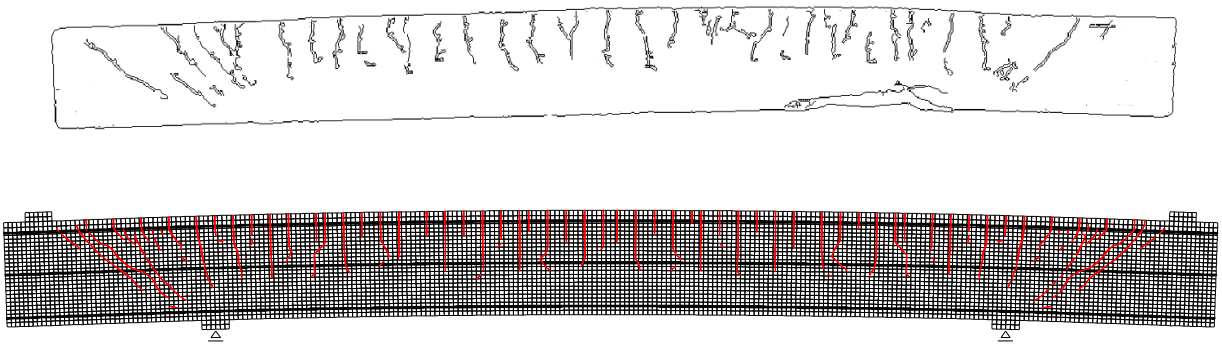

(b)

Figure 6. Comparison between experimental and numerical crack patterns at final stage of loading for specimen: (a) 12-20-00; and (b) 25-20-00.

The first principle stress is represented in Figure 7 using a colour scheme that highlights the stresses in concrete and that shows the role of active cracks in the dissipation of tensile stresses. The tension stiffening effect is evident with the concrete between cracks being able to withstand a certain amount of tensile stress. Closer to the crack this stress becomes zero (blue colour) due to the equilibrium conditions between crack and concrete mentioned in section 2.

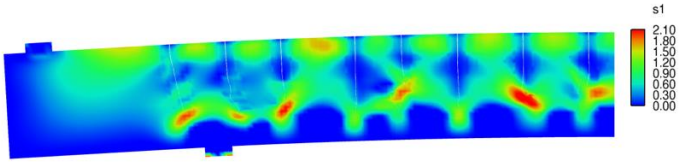

Figure 7. First principle stress map at 70kN (displacements magnified by a factor of 10).

4. Conclusions

This paper presented a preliminary study that is part of a research plan aimed at assessing the error of numerical models in the estimation of crack openings and average spacing. This first part of the study assessed the performance of the finite element model based on embedded discontinuities. The assumption underlying this model is that displacements caused by the opening of discontinuities induce a rigid body displacement on their neighbourhood. Experimental tests from Pérez Caldentey et al. [17]

provided data for average and maximum crack openings, and average crack spacing, for two concrete beams with different rebar diameters.

The overall crack pattern and main features of the model were shown to be correctly captured by the numerical model. The load vs. displacement of the concrete member was similarly captured using coarse and refined meshes, and good agreement was observed with available experimental results. The models further showed to be able to handle the process of debonding in the neighbourhood of cracks, which was critical to simulate the tension stiffening effect. The numerical load vs. displacement curves highlight the progressive loss of stiffness with increasing damage and deflections, and correctly predicted the load at the onset of cracking and subsequent typical stages of flexural behaviour.

Since only one discontinuity was allowed per finite element in the numerical implementation, coarser meshes were not always able to generate a single discontinuity crossing the entire depth of the beam. Instead, two or three partial cracks in the neighbourhood behave as if they were a single continuous crack, assuring that the energy is correctly dissipated. Although this could make the definition of average crack spacing harder for a coarse model, crack openings and patterns are generally well captured. When comparing with experimental results, the numerical models were shown to globally underestimate crack openings and spacing by an average error close to 30%. Since this error was of the same order for average and maximum crack openings, and average crack spacing, it was probably partially caused by a systematic source of error in the constitutive parameters that were not experimentally assessed. In particular, the fracture energy and the bond-slip law for steel reinforcements were not measured experimentally and both are highly relevant for the process of crack localisation and propagation.

5. Acknowledgement

The first author would like to acknowledge the support from the Australian Research Council through its Discovery Early Career Researcher Award (DE150101703) and Discovery Projects funding scheme (DP140100529), and from the Faculty of Engineering & Information Technologies, The University of Sydney, under the Faculty Research Cluster Program. Acknowledgment is also extended to FCT (Portuguese Foundation for Science and Technology), through ISISE, under project UID/ECI/04029/2013.

6. References

1. Bazant, Z., Oh, B.H., “Crack band theory for fracture of concrete”, Mater Struct, 16(3), 1983, pp 155–177.
2. Rots, J., “Smeared and discrete representations of localized fracture”, Int J Fracture, 51(1), 1991, pp 45–59.
3. Chong, K.T., Foster, S.J., Gilbert, R.I., “Time-dependent modelling of RC structures using the cracked membrane model and solidification theory”, Comput Struct, 86(11–12), 2008, pp 1305–1317.
4. Borst, R., Remmers, J., Needleman, A., Abellan, M.-A., “Discrete vs smeared crack models for concrete fracture: bridging the gap”, Int J Numer Anal Met, 28, 2004, pp 583–607.
5. Ingraffea, A.R., Saouma, V., “Numerical modelling of discrete crack propagation in reinforced and plain concrete”, Engineering Application of Fracture Mechanics, ed. G.C. Sih and A. Di Tommaso, M. Nijhoff Publishers, 4, 1985, pp 171–225.
6. Areias, P., Dias-da-Costa, D. et al. “Arbitrary Bi-Dimensional Finite Strain Crack Propagation”, Comput Mech, 45 (1), 2009, pp 61–75.
7. Ooi, E.T., Song, C. et al., “Automatic modelling of cohesive crack propagation in concrete using polygon scaled boundary finite elements”, Eng Fract Mech, 93, 2012, pp 13–33.
8. Duarte, C.A.M. J.T. Oden, “An h-p adaptive method using clouds”, Comput Method Appl M, 139(1-4), 1996, pp 237-262.
9. Belytschko, T., Gracie, R., Ventura, G., “A review of extended/generalized finite element methods for material modelling”, Model Simul Mater SC, 17(4), 2009, 1–24.

10. Simo, J.C. M.S. Rifai, “A class of mixed assumed strain methods and the method of incompatible modes”, Int J Numer Meth Eng, 29(8), 1990, pp 1595-1638.
11. Oliver, J., Cervera, M., Manzoli, O., “Strong discontinuities and continuum plasticity models: the strong discontinuity approach”, Int J Plasticity, 15(3), 1999, pp 319-351.
12. Alfaiate, J., Simone, A., Sluys, L.J., “Non-homogeneous displacement jumps in strong embedded discontinuities”. International Journal of Solids and Structures, 40(21), 2003, pp 5799-5817.
13. Alfaiate, J., L. J. Sluys, “On the use of embedded discontinuities in the framework of a discrete crack approach”, WCCM VI, Beijing, China, Tsinghua University Press & Springer-Verlag, 2004.
14. Dias-da-Costa, D., Alfaiate, J. et al., “A discrete strong discontinuity approach”. Engineering Fracture Mechanics, 76(9), 2009, pp 1176-1201.
15. Dias-da-Costa, D., Alfaiate, J. et al., “A Comparative Study on the Modelling of Discontinuous Fracture by Means of Enriched Nodal and Element Techniques and Interface Elements”, Int J Fracture, 161(1): 97–119, 2010.
16. Dias-da-Costa, D., Alfaiate, J. et al., “An embedded formulation with conforming finite elements to capture strong discontinuities”, Int J Numer Meth Eng, 93(2), 2013, 224–244 (doi: 10.1002/nme.4393).
17. Pérez Caldentey, A., Peiretti, H.C. et al., “Cracking of RC members revisited: influence of cover, $\phi / \rho_{s,ef}$ and stirrup spacing – an experimental and theoretical study”, Structural Concrete, 33(8), 2013, pp 2350-2356.
18. Hillerborg, A., Modéer, M., Petersson, P.-E., “Analysis of crack formation and crack growth in concrete by means of fracture mechanics and finite elements”, Cement and Concrete Research 6(6), 1976, pp. 773-781.
19. Malvern, L. E. “Introduction to the mechanics of a continuous medium”, Englewood Cliffs, New Jersey, Prentice-Hall International, 1969.
20. Goodman, R. E., et al. "A model for the mechanics of jointed rock." Journal of the Soil Mechanics and Foundations Division, 99, 1968, pp 637-659.
21. Graça-e-Costa, R., et al., “A non-iterative approach for the modelling of quasi-brittle materials”. International Journal of Fracture, 178(1-2), 2012, 281-298.
22. fib, “Model Code for Concrete Structures 2010”, Weinheim, Germany: Wiley-VCH Verlag GmbH & Co, KGaA, 2013.
23. Engen, M., Hendriks, M.A.N. et al. “Large scale non-~linear finite element analyses of reinforced concrete structures”, Proceedings, 10 th fib International PhD Symposium in Civil Engineering, 2014.
24. Cervenka, V., Markova, J. et al., “Uncertainties of crack width models”, Proceedings, fib Symposium 2017, Maastricht, The Netherlands, 2017.